Observed three-dimensional structure of a cold eddy in the southwestern South China Sea

Jianyu Hu,[1] Jianping Gan,[2] Zhenyu Sun,[1] Jia Zhu,[1] and Minhan Dai[1]

[1] The dynamic structure of an ocean eddy in the eddy-abundant South China Sea has rarely been captured by measurements and has seldom been discussed in the literature. In the present study, in situ current and hydrographic measurements from a weeklong cruise and concurrent satellite altimeter observations were utilized to examine the three-dimensional structure and physical properties of a cold eddy in the southwestern South China Sea. The underlying forcing mechanism for the formation of this cyclonic cold eddy was found to be tightly associated with the recirculation in a coastal baroclinic jet that had separated off the Vietnamese coast. The eddy was significantly influenced by a coexisting, anticyclonic warm eddy in the separated jet. With relatively steady intensity and radius, the cold eddy endured for two weeks after its swift formation in late August and prior to its quick dissipation in mid-September. This cold eddy was horizontally and vertically heterogeneous. Asymmetric currents with much stronger magnitude were found on its southeastern flank, next to the warm eddy, where a front in the pycnocline was responsible for the sharp decrease in the cold eddy's intensity in the water below. The distributions of temperature, vorticity, and vertical velocity in the cold eddy were spatially asymmetric and not overlapping. The intensity of the cold eddy gradually decreased with the depth and the eddy extended downward for more than 250 m with a vertically tilted central axis. The upward velocities around the center of the eddy and the downward velocities to the southwest and to the east of the center jointly formed the upward domes of isotherms and isohalines in the central part of the cold eddy.

Citation: Hu, J., J. Gan, Z. Sun, J. Zhu, and M. Dai (2011), Observed three-dimensional structure of a cold eddy in the southwestern South China Sea, *J. Geophys. Res.*, *116*, C05016, doi:10.1029/2010JC006810.

1. Introduction

[2] The South China Sea (SCS) (Figure 1) is a marginal sea with a central deep basin surrounded by shelves and islands. The ocean circulation of the SCS is jointly governed by Asian monsoon forcing, the Kuroshio intrusion, and the intrinsic dynamics involving topographic controls [e.g., *Qu*, 2000; *Hu et al.*, 2000; *Su*, 2001, 2004; *Gan et al.*, 2006]. Consequently, frontal instability, coastal jet separation and monsoon-driven forcing, abundant mesoscale eddies in the SCS greatly influence temporal and spatial variability of circulation [*Qu*, 2000; *Ho et al.*, 2000; *Chu and Fan*, 2001; *Wang et al.*, 2003a, 2003b, 2008; *Gan and Ho*, 2008; *Gan and Qu*, 2008; *Pullen et al.*, 2008; *Xiu et al.*, 2010].

[3] In summer, a northward coastal jet, forced by southwesterly wind stress, is formed over the narrow and steep shelf east of the Vietnamese coast. The jet detaches (or separates) from the Vietnamese coast at about 12°N [*Yuan et al.*, 2005], subsequently flows northeastward and carries the cold upwelled coastal waters into the interior of the SCS basin [*Xie et al.*, 2003]. This phenomenon was also observed in cruise data from 1989 to 1999 by *Fang et al.* [2002]. During the southwesterly monsoon period, the circulation in the southwestern SCS is often characterized by a dipole flow pattern, in which the separated coastal jet is sandwiched by an anticyclonic circulation in the south and a cyclonic circulation in the north [*Wang et al.*, 2006, *Gan and Qu*, 2008]. The coastal jet separation and the associated eddy formation are not only driven by the local dipole wind curl [*Kuo et al.*, 2000; *Xie et al.*, 2003; *Wang et al.*, 2006; *Cai et al.*, 2007; *Bayler and Liu*, 2008], but also governed by the boundary layer dynamics over the narrow shelf topography [*Gan and Qu*, 2008].

[4] In the open ocean, eddy formation is often associated with energy and vorticity inputs from atmospheric forcing. However, the intensity, endurance, and dissipation of an eddy are greatly controlled by its three dimensional structure as well, particularly the structure in the vertical direction. For example, diapycnal mixing followed by geostrophic adjustment [*McWilliams*, 1985] or baroc/lininc instability [*Badin et al.*, 2009] rather than wind forcing alone can be the major

[1]State Key Laboratory of Marine Environmental Science, College of Oceanography and Environmental Science, Xiamen University, Xiamen, China.
[2]Division of Environment and Department of Mathematics, Hong Kong University of Science and Technology, Hong Kong, China.
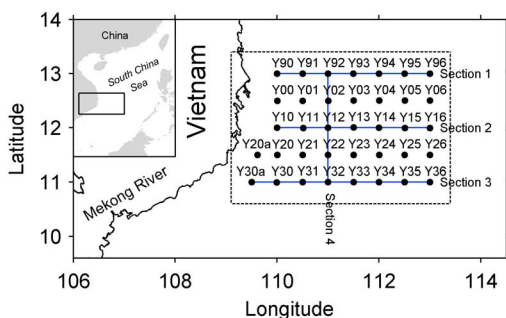
Figure 1. Conductivity-temperature-depth (CTD) stations in the southwestern South China Sea (SCS) during the early September cruise in 2007.

dynamic factors regulating the temporal and spatial scales of a geostrophic eddy in stratified waters. Baroclinic eddy has been observed off Sitka, Alaska [*Tabata*, 1982]. The eddies in the southwestern SCS govern the regional circulation during summer. Previous studies mainly focused on the surface feature of these eddies; the three-dimensional structure of the eddy that chiefly controls the dynamics remains poorly known. The eddies in the southwestern SCS are generally localized and induced by the local circulation associated with wind forcing [*Wang et al.*, 2003a, 2008; *Gan et al.*, 2006, *Gan and Qu*, 2008]. As a result of the intrinsic dynamics associated with the horizontal and vertical structures of these eddies, they tend to develop vertically to a water depth greater than O $(10^2$ m) and endure beyond the time scale of the wind forcing. There is little knowledge about the temporal and spatial variability within these eddies and this hinders the understanding of the eddy dynamic process as well as the regional circulation. On the basis of the analyses of in situ current, hydrographic measurements and concurrent satellite observations, this study describes the three-dimensional dynamic structure that is important in the development, sustenance, and dissipation of cold eddies in the ocean.

2. Data and Methods

[5] A field cruise on the ship, R/V *Dongfanghong 2*, was conducted in the southwestern SCS in early September 2007. The cruise consisted of three cross-shore transects (marked as sections 1, 2, and 3 in Figure 1), and an along-shore transect (section 4). The temperature and salinity were measured at each station using either an SBE 911 conductivity-temperature-depth (CTD) profiler or an SBE 917 plus CTD profiler manufactured by the Sea Bird Corporation. During the cruise, a shipboard acoustic Doppler current profiler (ADCP) was used for underway measurements of the currents.

[6] The satellite altimeter data used in this study were obtained from the Global Near Real-Time Sea Level Anomaly (SLA) Data Viewer at the Colorado Center for Astrodynamics Research (CCAR) at the University of Colorado, Boulder. This study used the analysis products that were generated based on the most recent 10 d of Jason and Topex/Poseidon, 17 d of Geosat Follow-On, and 35 d of European Remote Sensing Satellites (ERS 2 and Envisat) sampling. From the

merged altimeter data, the SLA distribution and the associated geostrophic current were obtained.

3. Eddy Evolution Detected by Satellite Altimeter Data

[7] During the survey period, the existence of a strong coastal jet characterized the circulation in the southwestern SCS (Figure 2). The jet formed a dipole recirculation pattern and flowed northeastward between a cyclonic cold eddy (hereafter referred to as C2) and an anticyclonic warm eddy (hereafter referred to as W2). Interestingly, the jet's path was not along the contour of zero wind curl, which was expected because of the Sverdrup relation, and the centers of C2 and W2 were not correlated with the respective maximum and minimum values of wind stress curl. Clearly, boundary layer dynamics [*Gan and Qu*, 2008] rather than wind stress curl alone governed the jet separation in the region. Temporally, C2 became apparent on 26 August, reached its peak intensity (the lowest SLA) at the beginning of September, and dissipated thereafter (Figure 3). The horizontal scale of C2 was about 60 ~ 90 km and lasted for about 2 weeks from 26 August to 10 September 2007. C2 moved slightly eastward at its onset stage from 26 to 28 August, but was stably centered on (110.8°E, 12.2°N) afterward. The intensity of C2 was relatively steady during its mature stage, while the rapid intensification/dissipation within 1 to 2 d occurred during onset and in the final stages. The underlying forcing mechanism for these quick transitions is not clear.

4. Hydrographic Structure of the Cold Eddy

4.1. Temperature Field in the Eddy

[8] We conducted the CTD mapping and underway ADCP profiling from 2 to 8 September in 2007 when C2 was well-developed (Figure 4). The sampling was conducted at a spatial interval of 50 ~ 60 km horizontally. Figure 4 shows the temperature distribution in C2 and its surrounding water at different depths. In the surface and in the 10 m layer, the survey area was covered with nearly homogeneous warm water (Figures 4a and 4b) and the cold core of C2 was invisible. At 20 m, an isotherm with temperature <26°C enclosed the cold core. The core temperature was about 2 to 3°C lower than that of the surrounding water (Figure 4c). An eddy-like isotherm with the lowest temperature centered at (110.8°E, 12.2°N) became apparent at 25 m with a diameter of about 100 ~ 150 km (Figure 4d). The cold eddy was well-developed at 50 m and the cold core temperature (<20°C) was about 8°C lower than that of the eastern surrounding water (Figure 4e). Unlike conditions in the upper layer, the deeper eddy was distinctly flanked by the warm water along both its southern and eastern borders, which formed a strong temperature front. The temperature structure of the cold eddy at 75 m or 100 m was almost the same as that at 50 m, and the temperatures were close to 18°C (Figure 4f) at 75 m, and lower than 17°C at 100 m (Figure 4g), respectively. The temperature front had the strongest intensity at about 50 m and was weaker below and above. It was clearly associated with the contrasting water temperature between C2 and W2 in the pycnocline. The temperature in the core of C2 gradually decreased and reached to less than 10°C
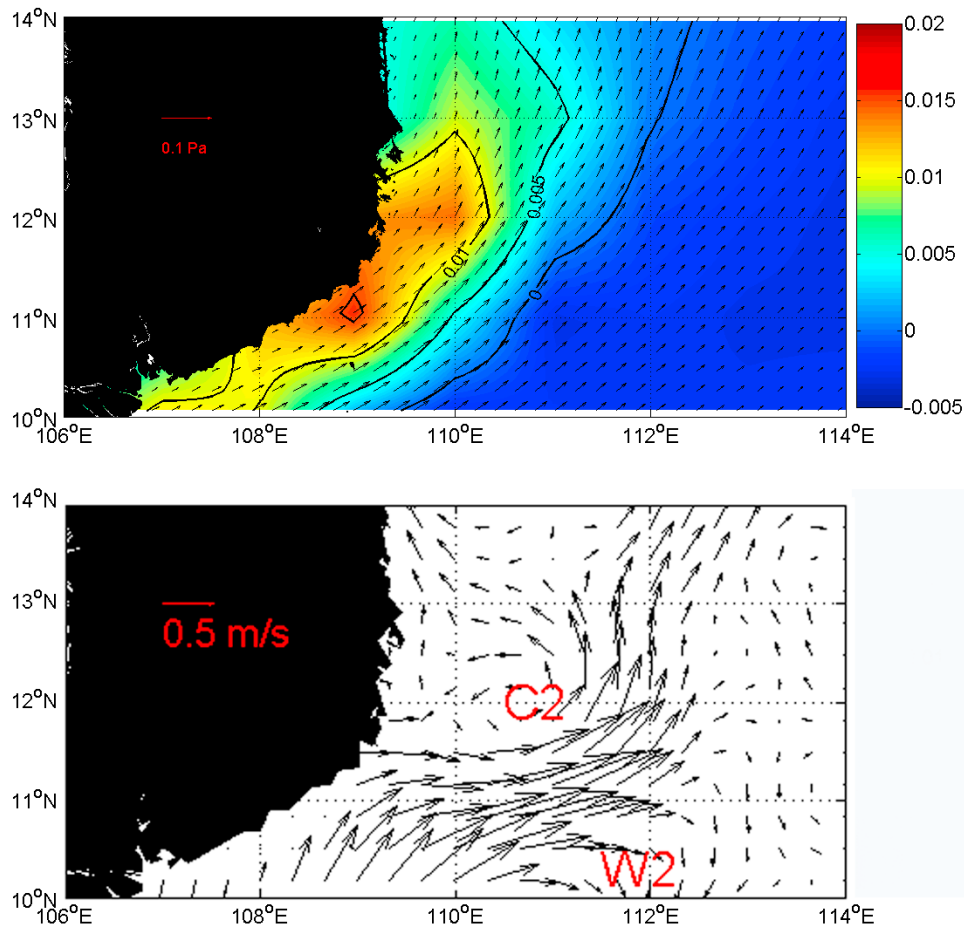
Figure 2. (top) Wind stress curl from NCEP data (National Center for Environmental Prediction, http://www.ncep.noaa.gov/) and (bottom) AVISO (Archiving, Validation and Interpretation of Satellite Oceanographic data, http://www.aviso.oceanobs.com/duacs/) surface absolute geostrophic currents averaged from 24 August to 10 September 2007. Cyclonic cold and anticyclonic warm eddies are marked C2 and W2, respectively.

at 400 m while the temperature front was quickly fading. C2 eventually disappeared in the 500 m layer (Figure 4l), but was able to penetrate more deeply than W2. The front led to a velocity vertical shear that reduced the velocity beneath it according to thermal wind relation (as shown in Figures 5 and 7), and may have been crucial to the eddy's circulation in the depths between 50 and 100 m where the pycnocline existed. Absences of both horizontal and vertical temperature gradients in the mixed upper layer and the layer below the pycnocline were dynamically unfavorable for the baroclinic eddy in either of those layers.

4.2. Salinity Field in the Eddy

[9] The salinity distribution (Figure 5) is similar to the temperature distribution except in the upper layer where the Mekong River plume intruded along the jet between C2 and W2. Analog to the surface temperature in which air-sea interaction and wind-induced mixing horizontally and vertically eroded the eddy's thermal signals, the surface salinity was largely modulated by the plume water intrusion.

In the surface layer, tongue-like low-salinity water (salinity <31.5) appeared in the southwestern corner of the survey area (Figure 5a) and penetrated to 25 m (Figures 5b–5d). The salinity field at the edge of the C2 was likely modified by the horizontal entrainment of the northeastward river plume (Figures 5a–5e), which moved the high-salinity center in the upper 25 m closer to the coast as compared to the corresponding low-temperature center in Figure 4 and the low SLA in Figure 3. Between the high-salinity water of C2 and the plume water farther south, there existed a clear west–east salinity front and that extended from the surface to the 25 m layer (Figures 5a–5d). Between 50 m and 100 m (Figures 5e–5g), a southwest–northeast salinity front was formed between C2 and W2. Similar to what occurred in the temperature field, the salinity field suggested that the influence of W2 weakened and the front disappeared below 150 m (Figures 5h–5j). At 400 m and 500 m, the salinity was spatially homogeneous with a value of about 34.44 (Figures 5k and 5l), similar to the feature of temperature distribution.
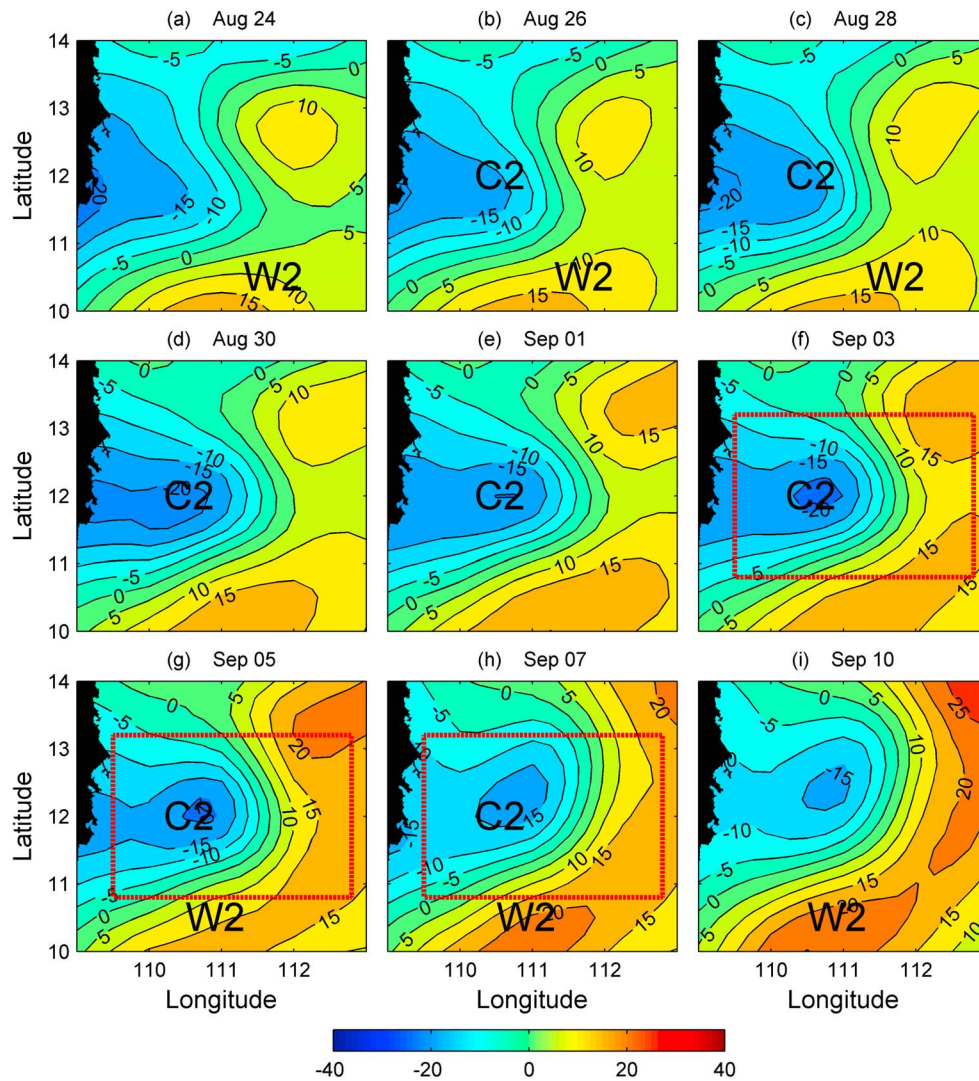
Figure 3. Evolution of eddies off the Vietnamese coast in the southwestern SCS, detected by satellite altimeter sea level anomaly (SLA) data, from 24 August to 10 September 2007. The dashed red box denotes the CTD mapping area during the early September cruise in 2007: (a) 24 August, (b) 26 August, (c) 28 August, (d) 30 August, (e) 1 September, (f) 3 September, (g) 5 September, (h) 7 September, and (i) 10 September. C2 and W2 represent the cold eddy and the warm eddy, respectively. The SLA distributions shown in Figures 3f, 3g, and 3h occurred during 2–8 September 2007.

4.3. Vertically Stratified Structure in the Eddy

[10] The vertical structure of C2 is further displayed by the sectional temperature and salinity distributions along the three cross-eddy sections (Figure 6). Along all three sections, there was a low-temperature dome below 50 m. The most intense upward temperature dome occurred around 80–100 m where the slope of the isotherms was the steepest. The center of the dome shifted southwestward from section 1 toward section 3. A larger tilt of the center axis line occurred at section 3, similar to the orientation of the vertical axis of the eddy, as shown in Figures 4 and 5. The tilt was presumably caused by a strongly stratified water column partly because of the intrusion of river plume water. The thermocline in the central part of C2 was in the shallower position about 25 m below surface layer.

[11] Similarly, a high-salinity dome existed at the center of C2 but at deeper water below the surface layer. Unlike the temperature in the surface layer, the fresher river plume water tended to encircle the center of the salinity dome and partially penetrate into C2. As a result, a halocline formed between the warm fresh water in the surface layer and the cold salty water below; combined with thermocline, the pycnocline may provide potential energy for the development of C2.

4.4. Depth-Dependent Geostrophic Current

[12] Geostrophic currents were calculated at specific depths, with a reference depth of 1200 m, from the CTD data measured at the five sections (Figure 1). For water shallower than 1200 m, or if the CTD measurement did not reach 1200 m, a reference depth in the adjacent area was applied. Figure 7
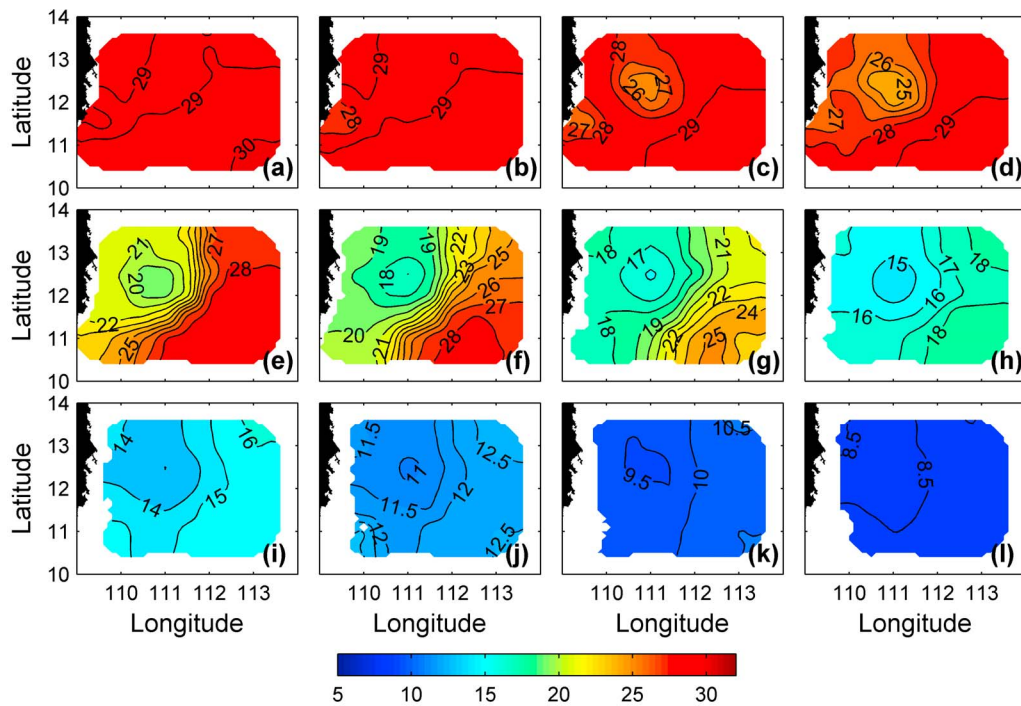
Figure 4. Temperature distribution in the southwestern SCS in early September 2007: (a) surface and (b) 10, (c) 20, (d) 25, (e) 50, (f) 75, (g) 100, (h) 150, (i) 200, (j) 300, (k) 400, and (l) 500 m.

shows that a distinctive cyclonic eddy existed from the surface layer down to 200 m. During the survey, the currents were directly measured by the ADCP from 25 m to 489 m at a vertical interval of 16 m. The geostrophic currents calculated from the CTD data agreed well with the measured ones in both magnitude and the direction (Figures 7d and 7f).

[13] The velocity field in C2 was horizontally asymmetric. Stronger currents, as high as 1.0 m s^{-1}, were distributed on
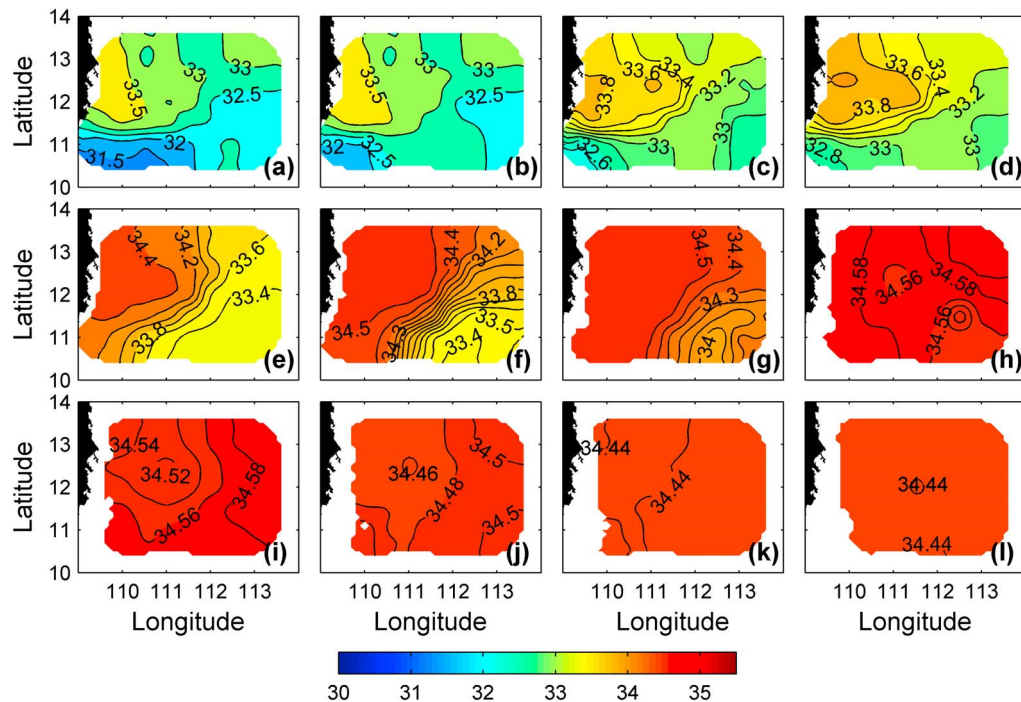

Figure 5. Salinity distribution in the southwestern SCS in early September 2007: (a) surface and (b) 10, (c) 20, (d) 25, (e) 50, (f) 75, (g) 100, (h) 150, (i) 200, (j) 300, (k) 400, and (l) 500 m.
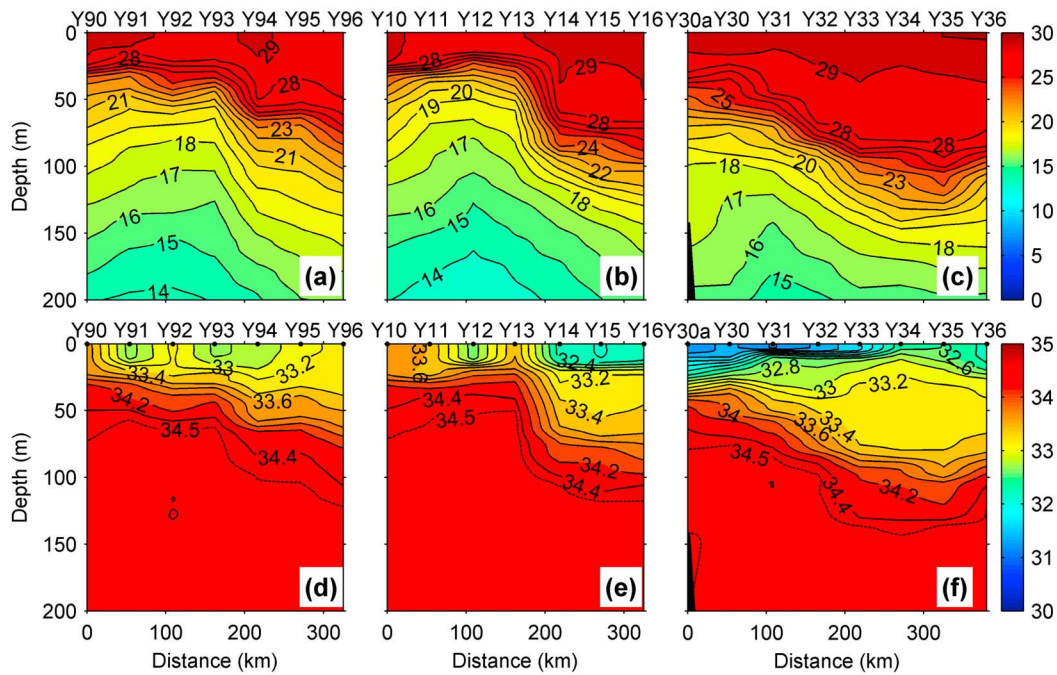
Figure 6. Sectional temperature and salinity distributions along three cross-shore sections in the southwestern SCS in early September 2007: temperature distributions along (a) section 1 (Y90–Y96), (b) section 2 (Y10–Y16), and (c) section 3 (Y30a–Y36) and temperature distributions as in Figures (d) 6a, (e) 6b, and (f) 6c but for salinity.
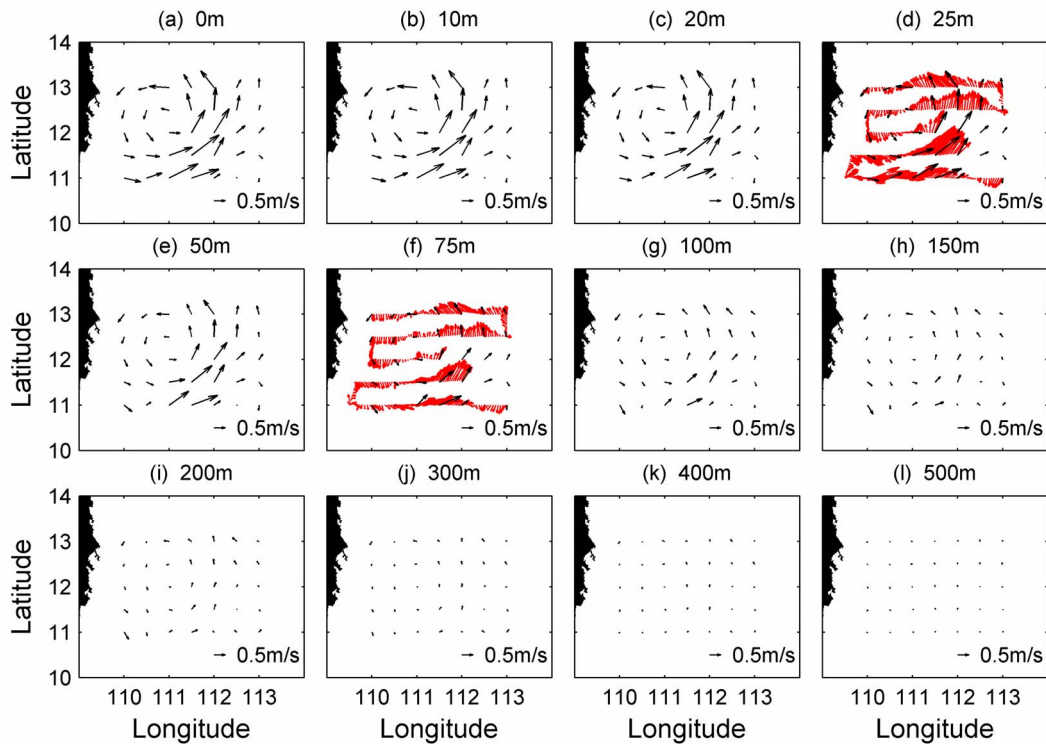

Figure 7. Geostrophic current field in the southwestern SCS in early September 2007: (a) surface and (b) 10, (c) 20, (d) 25, (e) 50, (f) 75, (g) 100, (h) 150, (i) 200, (j) 300, (k) 400, and (l) 500 m. Figures 7d and 7f show the current vectors measured by an acoustic Doppler current profiler (red) overlapping the geostrophic current calculated from CTD data (black).
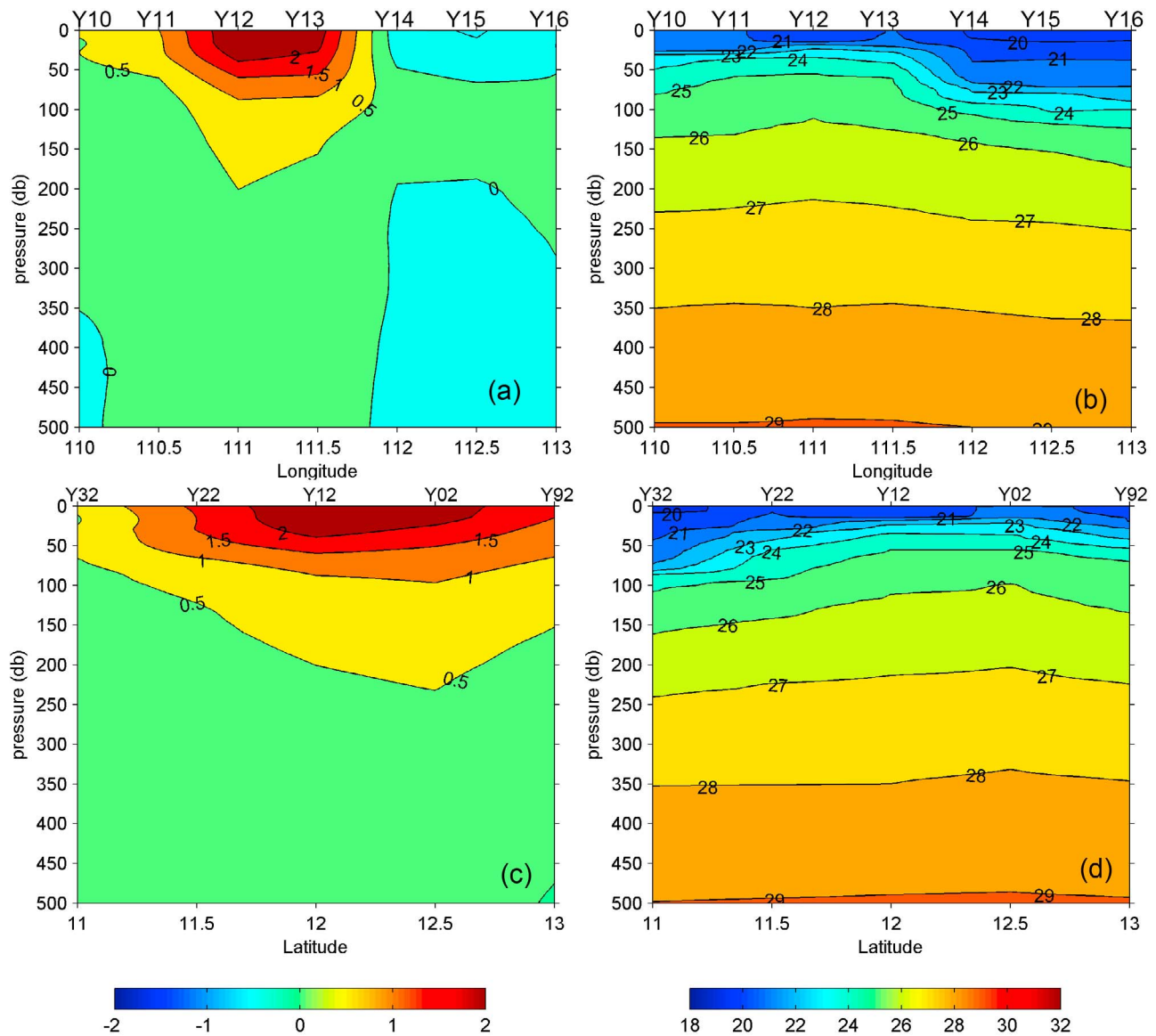
Figure 8. Sectional distributions of vorticity and density along sections 2 and 4: (a) vorticity and (b) density along section 2 (Y10–Y16) and (c) vorticity and (d) density along section 4 (Y32–Y92). The units of the current vorticity are 10^{-5} s^{-1}, and density is represented by the density anomaly (= density − 1000) with units of kg m^{-3}.

its southeastern side and weaker currents of 0.4 m s^{-1} were on its northwestern side (Figure 7a). The stronger currents were associated with the front between C2 and W2. Vertically, the eddy had a very similar velocity structure in the 10 m, 20 m, and 25 m layers (Figures 7b–7d), but the velocity gradually weakened below the 50 m layer where the strongest velocity was about 0.8 m s^{-1} (Figure 7e). The velocity of the coastal jet on the eastern flank of C2 quickly decreased to about 0.4 m s^{-1} at 150 m (Figure 7h), and the rapid weakening of the velocity between 50 m and 100 m is likely induced by the strong velocity vertical shear associated with the front (Figures 4, 5, and 6). Although the cyclonic pattern of the eddy still existed below 200 m, the velocity was very weak (Figures 7i–7l).

[14] The eddy's center derived from the current fields was well-matched with the location determined from the abso-

lute geostrophic currents (Figure 2) and SLA (Figure 3) as well as from the hydrographic analyses (Figures 4 and 5). An ensemble of these results evidently supports dynamic correlation between the separation of the coastal jet off Vietnam and C2 and W2 on the jet's northern and southern sides, respectively. Since C2's center deviated from the positive wind stress curl (Figure 2), it is conceivable that the C2 is not merely induced by the wind stress curl, but also largely associated with the recirculation in the jet stream. The mechanism of eddy formation in a separated coastal jet has also been shown by *Gan et al.* [1997, 2004].

5. Analysis and Discussion

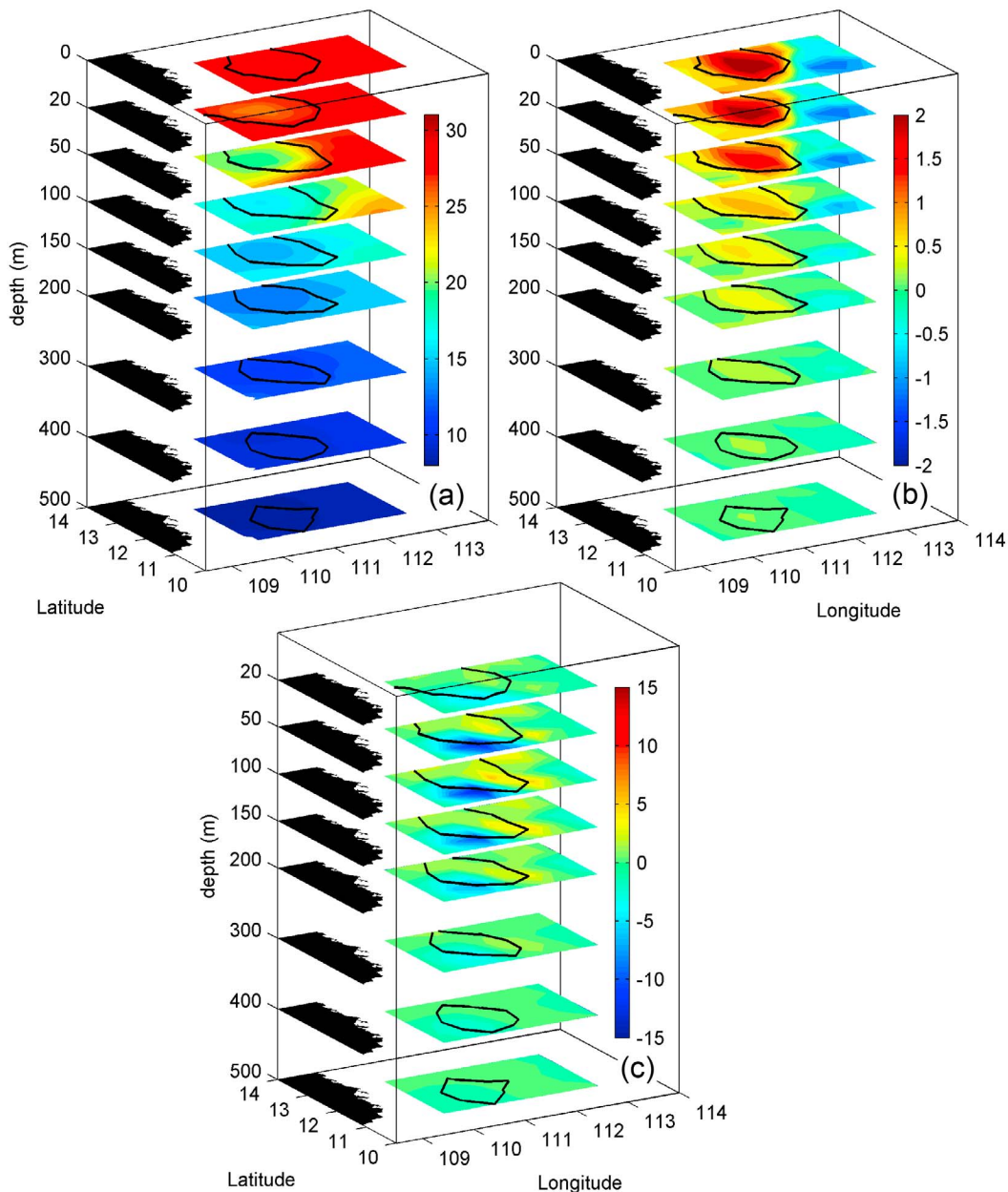[15] Figure 8 shows the geostrophic vorticity and the density across the center of maximum vorticity along sections 2

Figure 9. Three-dimensional structures of (a) temperature (°C), (b) vorticity (10^{-5} s^{-1}), and (c) vertical velocity (10^{-5} m s^{-1}, positive upward). The contour lines in black are those of the $-0.2\sigma_w$ that defines the scale of the eddy at each depth.

and 4. The maximum vorticity appeared in the surface layer between stations Y12 and Y13, where the center of C2 was located. The C2 extended vertically downward and its distinct feature is clearly identifiable to 200 m. In both sections, stronger upward domed density contours roughly occurred within the scope of the positive vorticity in the upper 200 m.

[16] In order to better specify physical properties within C2, we adopted the Okubo-Weiss parameter, W, with the following formula [*Isern-Fontanet et al.*, 2003; *Henson and Thomas*, 2008; *Gan and Ho*, 2008], to define the spatial scale of C2:

$$W = s_n^2 + s_s^2 - \omega^2, \qquad (1)$$

where vorticity (ω) and the normal (s_n) and shear (s_s) components of the strain are defined, respectively, as

$$\omega = \frac{\partial v}{\partial x} - \frac{\partial u}{\partial y}, \quad s_n = \frac{\partial u}{\partial x} - \frac{\partial v}{\partial y}, \quad s_s = \frac{\partial v}{\partial x} + \frac{\partial u}{\partial y}. \qquad (2)$$

Here (u, v) are the horizontal velocity components with positive values directed eastward (x) and northward (y), respectively. The eddy core is usually defined as a coherent region of negative W against a background field of small positive and negative W values. Following the criterion proposed by *Isern-Fontanet et al.* [2003], which was effectively used to define a stationary eddy by *Henson and Thomas* [2008], the
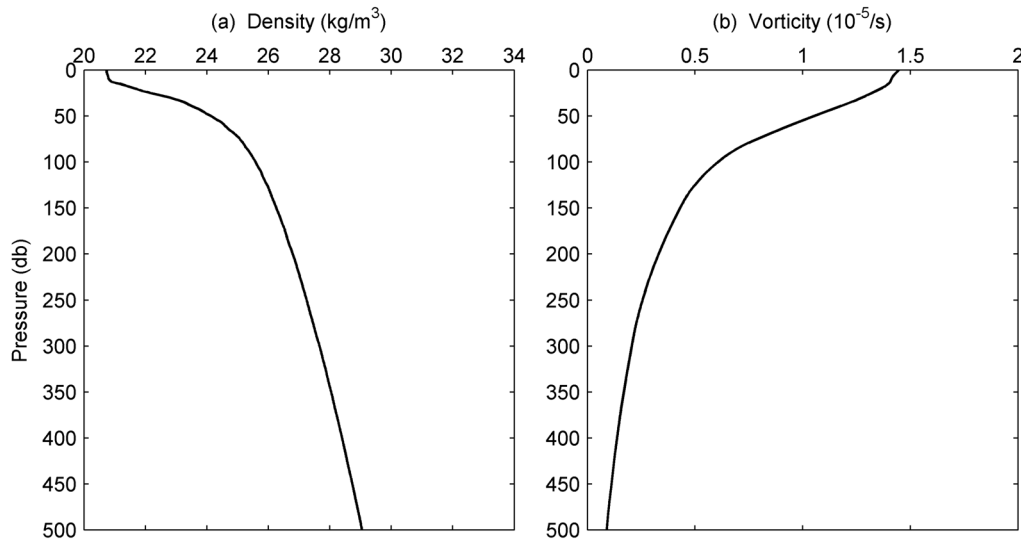
Figure 10. Vertical profiles of (a) density (kg m^{-3}) and (b) vorticity (10^{-5} s^{-1}) averaged in C2 defined by the Okubo-Weiss parameter. The density is represented by the density anomaly (= density − 1000).

eddy core threshold value of W was defined as $-0.2\sigma_w$, where σ_w is the standard deviation of W.

[17] Figure 9 demonstrates the three-dimensional structure of temperature, vorticity, and vertical velocity at representative depths. The vertical velocity, w, is obtained from the quasi-geostrophic (QG) Omega equation [e.g., *Martin and Richards*, 2001]:

$$f^2 \frac{\partial^2 w}{\partial z^2} + N^2 \left(\frac{\partial^2}{\partial x^2} + \frac{\partial^2}{\partial y^2} \right) w = \nabla_h Q$$

where Q is expressed as a vector

$$Q = \left[2f \left(\frac{\partial v_g}{\partial x} \frac{\partial u_g}{\partial z} + \frac{\partial v_g}{\partial y} \frac{\partial v_g}{\partial z} \right), -2f \left(\frac{\partial u_g}{\partial x} \frac{\partial u_g}{\partial z} + \frac{\partial u_g}{\partial y} \frac{\partial v_g}{\partial z} \right) \right]$$

(3)

and where f is the Coriolis parameter, N is the buoyancy frequency, and u_g and v_g are geostrophic velocities.

[18] The positive vorticity in C2 had a maximum at each of the selected depths (Figure 9). This value decreased sharply from >2.0×10^{-5} s^{-1} at the surface to <0.6×10^{-5} s^{-1} at 100 m followed by a relatively gentle decrease toward to 200 m. Meanwhile, there is a negative vorticity to the southeast of the positive vorticity in the water column, representing the warm eddy W2. The vorticity distribution had a consistent dipole pattern throughout the water column with the jet core located between the positive and negative vorticities of the dipole. Encircled by $W = -0.2\sigma_w$ (contour lines in Figure 9), the eddy radius R was about 90 km in the surface layer and decreased with a tilting eddy center axis with depth. The eddy radius, R, is estimated by $R = \sqrt{\frac{A}{\pi}}$, where A is an area encircled by the $-0.2\sigma_w$ contour. Relatively cold water at each level appeared mainly within the area of positive vorticity encircled within $W = -0.2\sigma_w$, but the location of the cold center did

not well overlap with the area of maximum vorticity and vertical velocity. The colder water in each layer of C2 appeared to the northwest of the larger vorticity. At the same time, the upward vertical velocity was generally linked with the positive vorticity within C2; but the downward velocity, occupied southwest quadrant of the eddy, was not well-correlated with the negative vorticity in W2. The upward velocities in the eddy also extended eastward beyond the eddy, while relative weak downward velocities existed farther east (Figure 9). According to (3), these vertical motions were governed by the divergence of vector Q, or the ageostrophic velocities due to nonlinear interaction of geostrophic current. Thus, the upward domes of the isotherms and isohalines across eddy C2 (Figures 6 and 8) can be jointly formed by the upward motion around the center of the eddy and downward motions to the west and to the east of the center.

[19] The overall depth-dependent feature of C2 is illustrated by characterized variables averaged within the eddy defined by the Okubo-Weiss parameter. The vertical profiles of density and vorticity are shown in Figure 10 and the corresponding profiles of radius and vertical velocity are displayed in Figure 11. The eddy-averaged vorticity had its maximum in the surface layer and quickly decreased over the pycnocline toward the 100 m layer. Vorticity was relatively small below 200 m and decreased to <0.25×10^{-5} s^{-1} below 500 m.

[20] The decrease of the eddy radius with depth was relatively slow compared with the sharp decrease of the vorticity with depth in the pycnocline (Figure 11). The eddy radius still had about 65 km at 500 m, even though its vorticity was decreased to less than 0.25×10^{-5} s^{-1}. The maximum upward/downward motion appeared at about 80 m in the pycnocline where ageostrophic current is expected to be larger because of stronger horizontal density gradient perturbed within the eddy. The vertical turbulent flux and the baroclinic instability might have triggered ageostrophy and vertical motion in the eddy. The complex forcing mechanism
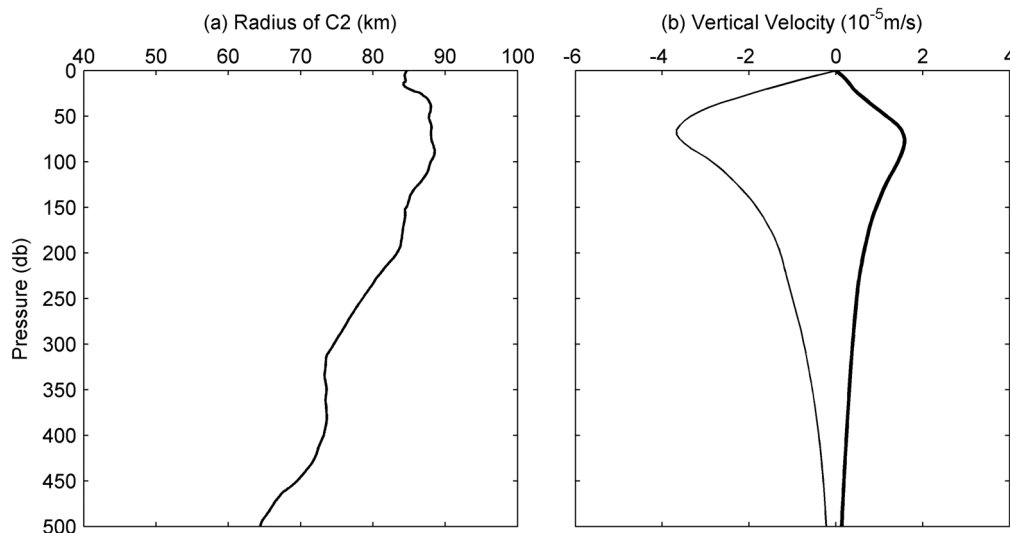
Figure 11. Vertical profiles of (a) eddy radius (km) and (b) upward (>0) and downward (<0) vertical velocities averaged within C2 defined by the Okubo-Weiss parameter.

for the vertical motion in the eddy in the southwestern SCS will be discussed in a separate study.

6. Summary and Conclusion

[21] In the southwestern SCS, the ocean circulation in summer is characterized by dipole eddies associated with coastal jet separation off the central Vietnamese coast. On the basis of CTD and ADCP in situ measurements and satellite altimeter observation, we presented the analysis of the three-dimensional dynamic structure of a cold eddy that has seldom been reported previously but is dynamically important.

[22] The cold eddy was formed quickly, within 2 d, near (110.8°E, 12.0°N) off central Vietnam in late August and it persisted for two weeks until mid-September before it dissipated in a short temporal scale of 2 d (Figure 3). This cold eddy was part of the recirculation in the separated coastal jet off Vietnam. In late August, the jet separated from the southern Vietnam coastal water and was sandwiched by the cold eddy and a warm eddy found on the northern and southern edges of the jet, respectively.

[23] The horizontal and vertical physical properties of the cold eddy during its mature stage were observed in the CTD mapping and the ADCP data. The eddy was highly heterogeneous in both horizontal and vertical directions. Horizontal asymmetric currents existed throughout the water column within the eddy with much stronger velocity in the southeastern side that neighbored the warm eddy. This asymmetric structure of the cold eddy was associated with a strong front along its southeastern flank in the pycnocline. Corresponding asymmetry was also seen in the vorticity and vertical velocity within the cold eddy. Relatively colder water at each layer of the eddy was located to the northwest of the greater vorticity and north of upward velocity. Both upward and downward motion existed within the cold eddy. The upward velocities around the center of the eddy and the downward velocities to the southwest and to the east of the center jointly formed the upward domes of isotherms and isohalines in the central part of the cold eddy. Strong

heterogeneity of vertical motion in the eddy is mainly induced by the ageostrophic velocities due to nonlinear interaction of geostrophic current, but the detailed dynamic forcing process remains largely unknown.

[24] Vertically, the intensity of the cold eddy was strongest in the surface and weakened sharply toward 100 m within the pycnocline. The axis of the eddy center tilted southwestward with depth, presumably because of the baroclinic effect in the vertically stratified eddy. The strongest upward/downward motion of the eddy was located just above the bottom of the pycnocline.

[25] This study filled the observational gap of the time-dependent three-dimensional dynamic structure of the eddy in the SCS. It also improved our understanding of eddy characteristics in the vertical transfer of energy, physical substance, nutrients and improved our understanding of eddy development, sustenance, and dissipation.

References

Badin, G., R. G. Williams, J. T. Holt, and L. J. Fernand (2009), Are mesoscale eddies in shelf seas formed by baroclinic instability of tidal fronts?, *J. Geophys. Res.*, *114*, C10021, doi:10.1029/2009JC005340.
Bayler, E. J., and Z. Liu (2008), Basin-scale wind-forced dynamics of the seasonal southern South China Sea gyre, *J. Geophys. Res.*, *113*, C07014, doi:10.1029/2007JC004519.
Cai, S., X. Long, and S. Wang (2007), A model study of the summer southeast Vietnam offshore current in the southern South China Sea, *Cont. Shelf Res.*, *27*, 2357–2372, doi:10.1016/j.csr.2007.06.002.
Chu, P. C., and C. Fan (2001), Low salinity, cool-core cyclonic eddy detected northwest of Luzon during the South China Sea Monsoon Experi-

ment (SCSMEX) in July 1998, *J. Oceanogr.*, *57*, 549–563, doi:10.1023/A:1021251519067.

Fang, W. D., G. H. Fang, P. Shi, Q. Z. Huang, and Q. Xie (2002), Seasonal structures of upper layer circulation in the southern South China Sea from in situ observations, *J. Geophys. Res.*, *107*(C11), 3202, doi:10.1029/2002JC001343.

Gan, J. and H. Ho (2008), Identification of spatial variability and eddies in the circulation of the South China Sea, in *Advances in Geosciences*, *Ocean Sci.*, vol. 12, edited by J. Gan, pp. 243–260, World Sci., Singapore.

Gan, J., and T. D. Qu (2008), Coastal jet separation and associated flow variability in the southwest South China Sea, *Deep Sea Res. Part I*, *55*, 1–19, doi:10.1016/j.dsr.2007.09.008.

Gan, J., R. Grant Ingram, and R. Greatbatch (1997), On the unsteady separation/intrusion of Gaspé Current and variability in Baie des Chaleurs: Modeling studies, *J. Geophys. Res.*, *102*, 15,567–15,581, doi:10.1029/97JC00589.

Gan, J., R. Grant Ingram, R. J. Greatbatch, and T. van der Baaren (2004), Variability of circulation induced by the separation of Gaspé Current in Baie des Chaleurs (Canada): Observational studies, *Estuarine Coastal Shelf Sci.*, *61*, 393–402, doi:10.1016/j.ecss.2004.06.009.

Gan, J., H. Li, E. N. Curchitser, and D. B. Haidvogel (2006), Modeling South China Sea circulation: Response to seasonal forcing regimes, *J. Geophys. Res.*, *111*, C06034, doi:10.1029/2005JC003298.

Henson, S. A., and A. C. Thomas (2008), A census of oceanic anticyclonic eddies in the Gulf of Alaska, *Deep Sea Res, Part I*, *55*, 163–176, doi:10.1016/j.dsr.2007.11.005.

Ho, C. R., Q. N. Zheng, Y. S. Soong, N. J. Kuo, and J. H. Hu (2000), Seasonal variability of sea surface height in the South China Sea observed with TOPEX/Poseidon altimeter data, *J. Geophys. Res.*, *105*, 13,981–13,990, doi:10.1029/2000JC900001.

Hu, J. Y., H. Kawamura, H. S. Hong, and Y. Q. Qi (2000), A review on the currents in the South China Sea: Seasonal circulation, South China Sea Warm Current and Kuroshio intrusion, *J. Oceanogr.*, *56*, 607–624, doi:10.1023/A:1011117531252.

Isern-Fontanet, J., E. Garcia-Ladona, and J. Font (2003), Identification of marine eddies from altimetric maps, *J. Atmos. Oceanic Technol.*, *20*, 772–778, doi:10.1175/1520-0426(2003)20<772:IOMEFA>2.0.CO;2.

Kuo, N. J., Q. N. Zheng, and C. R. Ho (2000), Satellite observation of upwelling along the western coast of the South China Sea, *Remote Sens. Environ.*, *74*, 463–470, doi:10.1016/S0034-4257(00)00138-3.

Martin, A. P., and K. J. Richards (2001), Mechanisms for vertical nutrient transport within a North Atlantic mesoscale eddy, *Deep Sea Res. Part I*, *48*, 757–773.

McWilliams, J. C. (1985), Submesoscale, coherent vortices in the ocean, *Rev. Geophys.*, *23*, 165–182, doi:10.1029/RG023i002p00165.

Pullen, J., J. D. May, C. Chavanne, P. Flament, and R. A. Arnone (2008), Monsoon surges trigger oceanic eddy formation and propagation in the lee of the Phillippine Islands, *Geophys. Res. Lett.*, *35*, L07604, doi:10.1029/2007GL033109.

Qu, T. D. (2000), Upper-layer circulation in the South China Sea, *J. Phys. Oceanogr.*, *30*, 1450–1460, doi:10.1175/1520-0485(2000)030<1450:ULCITS>2.0.CO;2.

Su, J. L. (2001), A review of circulation dynamics of the coastal oceans near China (in Chinese with English abstract), *Acta Oceanol. Sin.*, *23*, 1–16.

Su, J. L. (2004), Overview of the South China Sea circulation and its influence on the coastal physical oceanography outside the Pearl River Estuary, *Cont. Shelf Res.*, *24*, 1745–1760, doi:10.1016/j.csr.2004.06.005.

Tabata, S. (1982), The anticyclonic, baroclinic eddy off Sitka, Alaska, in the northeast Pacific Ocean, *J. Phys. Oceanogr.*, *12*, 1260–1282, doi:10.1175/1520-0485(1982)012<1260:TABEOS>2.0.CO;2.

Wang, G., J. Su, and P. C. Chu (2003a), Mesoscale eddies in the South China Sea observed with altimeter data, *Geophys. Res. Lett.*, *30*(21), 2121, doi:10.1029/2003GL018532.

Wang, G. H., R. F. Li, and C. X. Yan (2003b), Advances in studying oceanic circulation from hydrographic data with applications in the South China Sea, *Adv. Atmos. Sci.*, *20*, 914–920, doi:10.1007/BF02915514.

Wang, G., D. Chen, and J. Su (2006), Generation and life cycle of the dipole in the South China Sea summer circulation, *J. Geophys. Res.*, *111*, C06002, doi:10.1029/2005JC003314.

Wang, G., D. Chen, and J. Su (2008), Winter eddy genesis in the eastern South China Sea due to orographic wind jets, *J. Phys. Oceanogr.*, *38*, 726–732, doi:10.1175/2007JPO3868.1.

Xie, S. P., Q. Xie, D. X. Wang, and W. T. Liu (2003), Summer upwelling in the South China Sea and its role in regional climate variations, *J. Geophys. Res.*, *108*(C8), 3261, doi:10.1029/2003JC001867.

Xiu, P., F. Chai, L. Shi, H. Xue, and Y. Chao (2010), A census of eddy activities in the South China Sea during 1993–2007, *J. Geophys. Res.*, *115*, C03012, doi:10.1029/2009JC005657.

Yuan, Y. C., Y. G. Liu, G. H. Liao, R. Y. Lou, J. L. Su, and K. S. Wang (2005), Calculation of circulation in the South China Sea during summer of 2000 by the modified inverse method, *Acta Oceanol. Sin.*, *24*, 14–30.

M. Dai, J. Hu, Z. Sun, and J. Zhu, State Key Laboratory of Marine Environmental Science, College of Oceanography and Environmental Science, Xiamen University, Xiamen 361005, China.

J. Gan, Division of Environment and Department of Mathematics, Hong Kong University of Science and Technology, Hong Kong, China. (magan@ust.hk)